

Large Intelligent Surfaces for Energy Efficiency in Wireless Communication

Chongwen Huang, Alessio Zappone, *Senior Member, IEEE*,

George C. Alexandropoulos, *Senior Member, IEEE*,

Mérouane Debbah, *Fellow, IEEE*, and Chau Yuen, *Senior Member, IEEE*

Abstract

The adoption of Large Intelligent Surfaces (LIS) in assisting downlink multi-user communication from a multi-antenna base station is investigated in this paper. We present efficient designs for both the transmit power allocation and the coefficients of the surface reflecting elements, which target at maximizing either the energy or the spectral efficiency subject to individual link budget guarantees for the mobile users. Since both problem formulations are non-convex, we propose two computationally affordable approaches, which both capitalize on alternating maximization. To tackle the more demanding energy efficiency problem, we present an algorithm based on gradient descent for obtaining the LIS phase coefficients, while the optimal transmit power allocation is provided by a fractional programming method. For the energy efficiency maximizing LIS tuning, we also propose an efficient algorithm based on the majorization-minimization approach. Computer simulation results under a realistic outdoor system set up and power consumption model for LIS are presented, where LIS-assisted communication is extensively compared with the case of multi-antenna Amplify-and-Forward (AF) relaying. Our results corroborate the merits of LIS incorporation using both our proposed design algorithms, and it is indicated that LIS-assisted communication can provide up to 300% higher energy efficiency than the conventional AF relaying one.

Part of this work has been presented in *IEEE ICASSP*, Calgary, Canada, 14–20 April 2018 [1].

C. Huang and C. Yuen are with the Singapore University of Technology and Design, 487372 Singapore. (emails: chongwen_huang@mymail.sutd.edu.sg, yuenchau@sutd.edu.sg)

A. Zappone is with CentraleSupélec, University Paris-Saclay, 91192 Gif-sur-Yvette, France. (email: alessio.zappone@12s.centralesupelec.fr)

G. C. Alexandropoulos and M. Debbah are with the Mathematical and Algorithmic Sciences Lab, Paris Research Center, Huawei Technologies France SASU, 92100 Boulogne-Billancourt, France. M. Debbah is also with CentraleSupélec, University Paris-Saclay, 91192 Gif-sur-Yvette, France. (e-mails: {george.alexandropoulos, merouane.debbah}@huawei.com)

Index Terms

Large intelligent surfaces, multi-user MIMO, energy efficiency, spectral efficiency, non-convex optimization, alternating maximization, gradient descent, fractional programming, majorization-minimization.

I. INTRODUCTION

The highly demanding data rate requirements of emerging and future wireless networks (5-th Generation (5G) and beyond) have raised serious concerns on their energy consumption [2], [3]. These networks are anticipated to connect over 50 billions of wireless capability devices by 2020 [4] via dense deployments of multi-antenna base stations and access points [5]–[7]. As a consequence, the bit-per-Joule Energy Efficiency (EE) has emerged as a key performance indicator to ensure green and sustainable wireless networks [2], [3], [8], and several energy efficient wireless solutions have been proposed. A survey on the different approaches to implement energy efficient 5G wireless networks has recently appeared in [9]. Therein, the authors conclude that the energy challenge can be conquered only by the joint use of multiple approaches ranging from the use of renewable energy sources, energy efficient hardware components and relevant deployment techniques, as well as green resource allocation and transceiver signal processing algorithms. The issue of radio resource allocation for EE maximization in wireless networks is addressed in detail in [10], where the related mathematical tools are discussed.

Among the recent transceiver hardware technologies [11]–[13] with significant potential in reducing the energy consumption of wireless networks, while being theoretically capable of offering unprecedented massive Multiple-Input Multiple-Output (MIMO) gains [14]–[17], belong the Large Intelligent Surfaces (LIS). These surfaces are man made structures that can be electronically controlled with integrated electronics and wireless communication. A LIS usually comprises of a vast amount of small and nearly passive reflecting elements with reconfigurable parameters. Current implementations of LIS include conventional reflectarrays [11], [18], [19] and metasurfaces comprised of either liquid crystals [20], ferro-electric films, or other software defined metamaterials [21]. The LIS reflecting elements are usually very low cost and energy consumption units whose tuning may affect the electromagnetic behavior of the wireless propagation channel. Each of these units can effectively reflect a phase shifted version of the impinging electromagnetic field, hence, the combined configurations of all LIS elements may achieve certain communication objectives (e.g., synthesize pencil beams or enrich channel multipath).

Although LIS operation resembles that of a multi-antenna relay [22]–[25], it is fundamentally different from relaying communication. An intelligent surface is intended to perform as a scatterer with reconfigurable characteristics, and does not require any dedicated energy source for either decoding, channel estimation, and/or transmission. The unit cells in reflectarrays are usually patches that employ varactor diodes or other Micro-Electrical-Mechanical Systems (MEMS), and whose resonant frequency is electronically controlled [11]. Metasurfaces, on the other hand, consist of single- or few-layer stack of planar structures that can be readily fabricated using lithography and nanoprinting methods. Each of their unit patch elements is manipulated by varying the dielectric constant of the substrate [21]. Such low hardware footprint structures can be easily placed into buildings facades, room and factory ceilings, and laptop cases, up to being integrated into human clothing. Thus, multiple intelligent surfaces can be easily integrated in the communication environment with significant potential in improving coverage, overcoming unfavorable propagation conditions, and providing path diversity, while at the same time requiring much limited energy consumption than active relays and distributed antenna systems [26].

The design of LIS parameters for various communication objectives has started attracting research interest only very recently, focusing primarily on indoor environments. In [27], a $0.4m^2$ and $1.5mm$ thickness planar metasurface consisting of 102 controllable electromagnetic unit cells and operating at 2.47GHz was designed. Each unit cell is a rectangular patch sitting on a ground plane [28] and offering binary phase modulation. The metasurface was deployed as a spatial microwave modulator in a typical office room, and was demonstrated that it can passively increase the received signal power by an order of magnitude, or completely null it. Integrating each unit cell with one PIN diode in [29], a programmable metasurface with dynamic polarization, scattering, and focusing control was designed. The presented experiments demonstrated various controllable electromagnetic phenomena, including anomalous reflection and diffusion, as well as beamforming. A detailed analysis on the information transfer from multiple users to a LIS with active elements was carried out in [17], while [18] showed that a reflectarray can effectively improve data rates, while at the same time cancel interference. In this work, the results were also corroborated by measurements carried out on an office testbed. The role of LIS in improving indoor coverage was also analyzed in [30], [31]. Very recently, [19] experimented on the incorporation of a smart reflectarray in an IEEE 802.11ad network operating in the unlicensed 60GHz frequency band. In [21] the adoption of intelligent metasurfaces for actively reprogramming communication environments is envisioned, and its advantages in terms

of coverage, energy saving, and security are discussed. LIS with infinite phase resolution elements was considered in [1], where it was shown that higher Spectral Efficiency (SE) can be achieved when LIS-assisted communication is a feasible option. Adopting an exhaustive search approach, [32] showed that LIS structures with low phase resolution can obtain significant EE gains compared to conventional relay-assisted communication.

In contrast to previous literature, this work proposes two novel computationally affordable algorithms addressing the maximization of the bit-per-Joule EE of LIS-based systems, thus analyzing for the first time the energy gains that the use of LIS with infinite phase resolution elements can grant. In addition, unlike previous contributions, the analysis is carried out with reference to outdoor multi-user communication, considering a downlink Multiple Input Multiple Output (MISO) channel, thus for the first time studying the performance of LIS over longer distances. Specifically, the main contributions of this paper are summarized as follows.

- We present a convenient signal model for the considered LIS-assisted communication and describe a realistic LIS power consumption model that is based on the number of deployed reflector units and their phase resolution capability.
- We formulate the EE maximization problem under maximum power and minimum Quality of Service (QoS) constraints for the LIS-assisted downlink multi-user MISO scenario. Our design variables are the Base Station (BS) transmit powers for the multiple users and the optimum settings for the LIS reflecting elements.
- The EE maximization problem is non-convex and does not lend itself to be solved by standard approaches. Thus, we propose two computationally efficient algorithms merging alternating maximization, sequential fractional programming, conjugate gradient search and Majorization-Minimization (MM) optimization theories.
- We numerically evaluate the performance obtained through the proposed algorithms in a realistic set up. Our results indicate the merits of LIS-assisted communication, showcasing in particular that the use of LIS significantly improves the EE performance.

The remainder of this paper is organized as follows. In Section II, the multi-user MISO system assisted by reconfigurable LIS structures is described and the targeted EE maximization problem is formulated. The two derived algorithms for the EE maximization design are presented in Section III, and extensive numerically evaluated results are provided in Section IV. Finally, concluding remarks and future research directions are drawn in Section V.

Notation: a is a scalar, \mathbf{a} is a vector, and \mathbf{A} is a matrix. \mathbf{A}^T , \mathbf{A}^H , \mathbf{A}^{-1} , \mathbf{A}^+ , and $\|\mathbf{A}\|_F$ denote

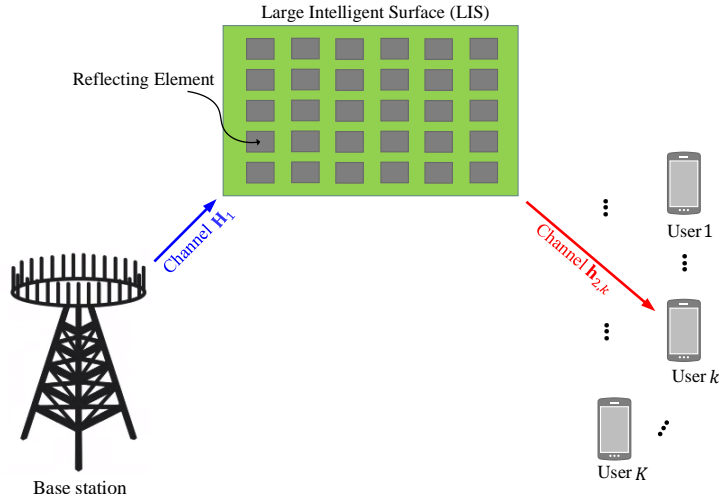


Figure 1. The considered LIS-assisted multi-user MISO system comprising of a M -antenna base station simultaneously serving in the downlink K single-antenna users. LIS is assumed to be attached to a surrounding building's facade, and the transmit signal propagates to the users via the assistance of LIS that is capable of reconfigurable behavior.

transpose, Hermitian (conjugate transpose), inverse, pseudo-inverse, and Frobenius norm of \mathbf{A} , respectively. $\text{Re}(\cdot)$, $\text{Im}(\cdot)$, $|\cdot|$, $(\cdot)^*$ and $\arg(\cdot)$ denote the real part, imaginary part, modulus, conjugate and the angle of a complex number, respectively. $\text{tr}(\cdot)$ denotes the trace of a matrix and \mathbf{I}_n (with $n \geq 2$) is the $n \times n$ identity matrix. $\mathbf{A} \circ \mathbf{B}$ and $\mathbf{A} \otimes \mathbf{B}$ denote the Hadamard and Kronecker products of \mathbf{A} and \mathbf{B} , respectively, while $\text{vec}(\mathbf{A})$ is a vector stacking all the columns of \mathbf{A} . $\text{diag}(\mathbf{a})$ is a diagonal matrix with the entries of \mathbf{a} on its main diagonal. $\mathbf{A} \succeq \mathbf{B}$ means that $\mathbf{A} - \mathbf{B}$ is positive semidefinite. Notation $x \sim \mathcal{CN}(0, \sigma^2)$ means that random variable x is complex circularly symmetric Gaussian with zero mean and variance σ^2 , whereas $E[x]$ denotes x 's expected value. \mathbb{R} and \mathbb{C} denote the complex and real number sets, respectively, and $j \triangleq \sqrt{-1}$ is the imaginary unit.

II. SYSTEM MODEL

In this section, we describe the signal model for the considered LIS-assisted downlink multi-user MISO system, and then present our adopted model for the system total power consumption. We also describe the targeted problem formulation for the joint design of the transmit powers for all users and the values for the LIS reflecting elements.

A. Signal Model

Consider the downlink communication between a BS equipped with M antenna elements and K single-antenna mobile users. We assume that this communication is realized via a LIS deployed on the facade of a building existing in the vicinity of both communication ends, as illustrated in Fig. 1. The direct signal path between the BS and the mobile users is neglected due to unfavorable propagation conditions. The LIS is equipped with $N \geq K$ nearly passive and cheap reflecting elements, each being capable of effectively applying a phase shift on the incoming electromagnetic field [11], [18]–[21], [30]–[33]. By suitably adjusting the LIS elements phase shifts, the intelligent surface can reconfigure the electromagnetic behavior of the wireless propagation channel according to desired objectives. Hence, LIS operation resembles more that of a reconfigurable scatterer than a relay impacting the propagation of the impinging information bearing signals.

The discrete-time signal received at mobile user k , with $k = 1, 2, \dots, K$, for the considered case of no direct signal path between the BS and any of the users can be written as

$$y_k \triangleq \mathbf{h}_{2,k} \mathbf{\Phi} \mathbf{H}_1 \mathbf{x} + w_k, \quad (1)$$

where $\mathbf{h}_{2,k} \in \mathbb{C}^{1 \times N}$ denotes the channel gain matrix between the LIS and user k , and $\mathbf{H}_1 \in \mathbb{C}^{N \times M}$ represents the channel between the BS and LIS. In addition, $\mathbf{\Phi} \triangleq \text{diag}[\phi_1, \phi_2, \dots, \phi_N]$ is a diagonal matrix accounting for the effective phase shifts applied by all LIS reflecting elements, where $\phi_n = e^{j\theta_n} \forall n = 1, 2, \dots, N$. The term $w_k \sim \mathcal{CN}(0, \sigma^2)$ is the thermal noise at user k , modeled as a realization of a zero-mean complex circularly symmetric Gaussian variable with variance σ^2 . Finally, $\mathbf{x} \triangleq \sum_{k=1}^K \sqrt{p_k} \mathbf{g}_k s_k$ denotes the transmitted signal with p_k , s_k , and $\mathbf{g}_k \in \mathbb{C}^{M \times 1}$ representing the transmit power, unit power complex valued information symbol chosen from a discrete constellation set, and precoding vector, respectively, intended for the k -th mobile user. For the expectation of the transmit signal power from the multi-antenna BS holds the maximum transmit power constraint:

$$E[|\mathbf{x}|^2] = \text{tr}(\mathbf{P} \mathbf{G}^H \mathbf{G}) \leq P_{\max}. \quad (2)$$

In the latter expression, $\mathbf{G} \triangleq [\mathbf{g}_1, \mathbf{g}_2, \dots, \mathbf{g}_K] \in \mathbb{C}^{M \times K}$, $\mathbf{P} \triangleq \text{diag}[p_1, \dots, p_K] \in \mathbb{R}^{K \times K}$, and P_{\max} denotes the maximum feasible transmit power.

As seen from the signal model of (1) for the considered multi-user MISO system, the reflecting surface is modeled as a scatterer with reconfigurable characteristics. It effectively applies the

phase shifting operation described by Φ to the impinging information bearing signal expressed by $\mathbf{H}_1\mathbf{x}$. In fact, LIS does not require any dedicated energy source for either decoding, channel estimation, or transmission [11], [18], [19], [30], [31]. This operation is fundamentally different from relays that consist of active antenna elements and generally perform energy consuming digital signal processing tasks. Getting back to (1), the Signal-to-Interference-plus-Noise Ratio (SINR) experienced at the k -th mobile user of the LIS-assisted system in Fig. 1 is obtained as

$$\gamma_k \triangleq \frac{p_k |\mathbf{h}_{2,k} \Phi \mathbf{H}_1 \mathbf{g}_k|^2}{\sum_{i=1, i \neq k}^K p_i |\mathbf{h}_{2,k} \Phi \mathbf{H}_1 \mathbf{g}_i|^2 + \sigma^2}. \quad (3)$$

The latter expression can be straightforwardly used for the computation of the system achievable sum rate performance in bps/Hz as

$$\mathcal{R} \triangleq \sum_{k=1}^K \log_2(1 + \gamma_k). \quad (4)$$

B. Total Power Consumption Model

The total power dissipated to operate our considered LIS-assisted system is composed of the BS transmit power, as well as the hardware static power consumed in the BS, mobile user terminals, and the intelligent surface. In particular, it should be stressed that the LIS does not consume any transmit power, since its reflectors are passive elements that do not directly alter the magnitude of the incoming signal. In fact, LIS has the potential of offering large beamforming gain to the mobile users, if the phases of the reflecting elements are appropriately adjusted. As previously mentioned, this is a significant difference compared to relay architectures [34], which instead consume Radio Frequency (RF) transmit power to process (e.g., Amplify-and-Forward (AF), decode-and-forward, and compress-and-forward) the incoming signal.

Putting all above together, the power consumption of the k -th wireless link (i.e., the LIS-assisted link between BS and the k -th mobile user) can be expressed as

$$\mathcal{P}_k \triangleq \xi p_k + P_c + P_{\text{LIS}}, \quad (5)$$

where $\xi \triangleq \nu^{-1}$ with ν being the efficiency of the transmit power amplifier, while P_c incorporates the hardware static power dissipated in all other circuit blocks of the BS and user equipments. Finally, P_{LIS} denotes the static power dissipated by the LIS. We should remark that the two underlying assumptions in (5) are: *i*) the transmit amplifier operates in its linear region; and *ii*) the circuit power P_c does not depend on the communication rate. Both assumptions are met in

typical wireless communication systems, which are operated so as to ensure that the amplifiers operate in the linear region of their transfer function, and in which the hardware-dissipated power can be approximated by a constant power offset.

To further specify the individual hardware power consumption terms in (5), we first express the circuit dissipated power at the active terminals as $P_c \triangleq P_{\text{BS}} + KP_{\text{UE}}$, where P_{BS} and P_{UE} denote the power consumptions at BS and each mobile user, respectively. The LIS power consumption depends on the type and the resolution of its individual reflecting elements that effectively perform phase shifting on the impinging signal. By assuming that each elements is actually a phase shifter, typical values of its consumed power are 1.5, 4.5, 6, and 7.8mW for 3-, 4-, 5-, and 6-bit resolution phase shifting [35], [36]. In the latter power values, the power consumption of the low noise amplifier has also been included. Therefore, the power dissipated at an intelligent surface with N identical reflecting elements can be written as $P_{\text{LIS}} = NP_n(b)$, where $P_n(b)$ denotes the power consumption of each phase shifter having b -bit resolution. Using the latter definitions, the total amount of power needed to operate the LIS-assisted downlink multi-user MISO system is given by

$$\mathcal{P}_{\text{total}} = \xi \sum_{k=1}^K p_k + P_{\text{BS}} + KP_{\text{UE}} + NP_n(b). \quad (6)$$

C. Design Problem formulation

We are interested in the joint design of the transmit powers for all users, included in $\mathbf{P} = \text{diag}[p_1, p_2, \dots, p_K]$, and the values for the LIS elements, appearing in the diagonal of $\Phi = \text{diag}[\phi_1, \phi_2, \dots, \phi_N]$, that jointly maximize the bit-per-Joule EE performance for the considered LIS-assisted system. This performance is defined as the ratio between the system achievable sum rate in bps and the total power consumption in Joule, i.e., $\eta_{\text{EE}} \triangleq \text{BWR}/\mathcal{P}_{\text{total}}$ with BW being the transmission bandwidth, and can be obtained using (4) and (6) as

$$\eta_{\text{EE}} = \frac{\text{BW} \sum_{k=1}^K \log_2(1 + \gamma_k)}{\xi \sum_{k=1}^K p_k + P_{\text{BS}} + KP_{\text{UE}} + NP_n(b)}. \quad (7)$$

The EE maximization will be carried out enforcing maximum power constraints as well as individual QoS requirements for all K mobile users. To make the targeted problem more tractable, we assume that: *i*) the reflectors phase shifting resolution is infinite, i.e., $2^b \gg 1$; and *ii*) all involved channels are perfectly known at BS that employs Zero-Forcing (ZF) transmission, which is known to be optimal in the high-SINR regime [37]. Note that the practical estimation (either

partial or explicit) of especially $\mathbf{h}_{2,k} \forall k = 1, 2, \dots, K$ and \mathbf{H}_1 is a difficult task that will require considering sophisticated methods (e.g., [38], [39]); this is left as future work.

The ZF precoding matrix whose columns appear in (1) is given by $\mathbf{G} = (\mathbf{H}_2 \Phi \mathbf{H}_1 + \mathbf{H})^+$, where $\mathbf{H} \triangleq [\mathbf{h}_{1,1}^T, \mathbf{h}_{1,2}^T, \dots, \mathbf{h}_{1,K}^T]^T \in \mathbb{C}^{K \times M}$ and $\mathbf{H}_2 \triangleq [\mathbf{h}_{2,1}^T, \mathbf{h}_{2,2}^T, \dots, \mathbf{h}_{2,K}^T]^T \in \mathbb{C}^{K \times N}$. Substituting this \mathbf{G} in (3), the considered EE maximization problem is expressed as follows¹:

$$\max_{\Phi, \mathbf{P}} \frac{\sum_{k=1}^K \log_2(1 + p_k \sigma^{-2})}{\xi \sum_{k=1}^K p_k + P_{\text{BS}} + K P_{\text{UE}} + N P_n(b)} \quad (8a)$$

$$\text{s.t. } \log_2(1 + p_k \sigma^{-2}) \geq R_{\min,k} \forall k = 1, 2, \dots, K, \quad (8b)$$

$$\text{tr}((\mathbf{H}_2 \Phi \mathbf{H}_1 + \mathbf{H})^+ \mathbf{P} (\mathbf{H}_2 \Phi \mathbf{H}_1 + \mathbf{H})^{+H}) \leq P_{\max}, \quad (8c)$$

$$|\phi_n| = 1 \forall n = 1, 2, \dots, N, \quad (8d)$$

where $R_{\min,k}$ in constraint (8b) denotes the individual QoS constraint of the k -th user. Also, constraint (8c) ensures that the BS transmit power is kept below the maximum feasible threshold P_{\max} , while constraint (8d) accounts for the fact that each LIS reflecting element can only provide a phase shift, without amplifying the incoming signal.

The optimization problem (8) is non-convex due to the presence of Φ to be optimized. In the sequel, we present two computationally efficient approaches to obtain our optimized design parameters.

III. ENERGY EFFICIENCY MAXIMIZATION

Solving the optimization problem described in (8) is challenging mainly due to the constraints (8c) and (8d). In order to develop a tractable algorithm for the design parameters, a convenient approach is to employ the alternating optimization technique [40] to separately and iteratively solve for \mathbf{P} and Φ . In particular, we first solve for Φ given a fixed \mathbf{P} , and then find the optimum \mathbf{P} when Φ is fixed. Iterating this process improves the EE value at each iteration step, and must eventually converge in the optimum value of the objective, since (8a) is upper-bounded on the feasible set. In the rest of this section, the optimization with respect to Φ for fixed \mathbf{P} , and with respect to \mathbf{P} for fixed Φ will be treated separately.

¹We have removed the constant BW from problem (8), which we will later on consider in the performance results.

A. Optimization with respect to the LIS Elements Values Φ

For a fixed transmit power allocation matrix \mathbf{P} , the design problem (8) becomes the following feasibility test:

$$\max_{\Phi} 1 \quad (9a)$$

$$\text{s.t. } \text{tr}((\mathbf{H}_2 \Phi \mathbf{H}_1)^+ \mathbf{P} (\mathbf{H}_2 \Phi \mathbf{H}_1)^{+H}) \leq P_{\max} \quad (9b)$$

$$|\phi_n| = 1 \quad \forall n = 1, 2, \dots, N. \quad (9c)$$

The challenge in solving problem (9) lies in the fact that its objective is non-differentiable and that (9c) is a non-convex constraint. To proceed further, we observe that (9) is feasible if and only if the solution of the following optimization problem:

$$\min_{\Phi} \text{tr}((\mathbf{H}_2 \Phi \mathbf{H}_1)^+ \mathbf{P} (\mathbf{H}_2 \Phi \mathbf{H}_1)^{+H}) \quad (10a)$$

$$\text{s.t. } |\phi_n| = 1 \quad \forall n = 1, 2, \dots, N \quad (10b)$$

is such that the objective can be made lower than P_{\max} .

Let us define $\Theta \triangleq \text{diag}[\theta_1, \theta_2, \dots, \theta_N]$ and then express Φ as the following function of Θ (recall that $\phi_n = e^{j\theta_n} \quad \forall n = 1, 2, \dots, N$): $\Phi(\Theta) = \text{diag}[e^{j\theta_1}, e^{j\theta_2}, \dots, e^{j\theta_N}]$. Using these definitions, problem (10) can be reformulated as the following unconstrained problem:

$$\min_{\Theta} \mathcal{F}(\Phi(\Theta)) \triangleq \text{tr}((\mathbf{H}_2 \Phi(\Theta) \mathbf{H}_1)^+ \mathbf{P} (\mathbf{H}_2 \Phi(\Theta) \mathbf{H}_1)^{+H}). \quad (11)$$

By expressing the power allocation matrix \mathbf{P} as $\mathbf{P} = \mathbf{Q}\mathbf{Q}^T$ with $\mathbf{Q} \triangleq \sqrt{\mathbf{P}}$, we observe that the objective function in (11) can be rewritten as

$$\begin{aligned} \mathcal{F}(\Phi(\Theta)) &= \text{tr}((\mathbf{H}_2 \Phi(\Theta) \mathbf{H}_1)^+ \mathbf{P} (\mathbf{H}_2 \Phi(\Theta) \mathbf{H}_1)^{+H}) \\ &= \text{tr}((\mathbf{Q}^{-1} \mathbf{H}_2 \Phi(\Theta) \mathbf{H}_1)^+ (\mathbf{Q}^{-1} \mathbf{H}_2 \Phi(\Theta) \mathbf{H}_1)^{+H}) \\ &\stackrel{a}{=} \text{tr}((\overline{\mathbf{H}}_2 \Phi(\Theta) \mathbf{H}_1)^+ (\overline{\mathbf{H}}_2 \Phi(\Theta) \mathbf{H}_1)^{+H}) \stackrel{b}{=} \|\mathbf{H}_1^+ \Phi^{-1}(\Theta) \overline{\mathbf{H}}_2^+\|_F^2 \\ &\stackrel{c}{=} \|\text{vec}(\mathbf{H}_1^+ \Phi^{-1}(\Theta) \overline{\mathbf{H}}_2^+)\|^2 = \|(\overline{\mathbf{H}}_2^{+H} \otimes \mathbf{H}_1^+) \text{vec}(\Phi^{-1}(\Theta))\|^2 \\ &= \text{vec}(\Phi^{-1}(\Theta))^H (\overline{\mathbf{H}}_2^{+H} \otimes \mathbf{H}_1^+)^H (\overline{\mathbf{H}}_2^{+H} \otimes \mathbf{H}_1^+) \text{vec}(\Phi^{-1}(\Theta)). \end{aligned} \quad (12)$$

In the latter expression, we have used the definition $\overline{\mathbf{H}}_2 \triangleq \mathbf{Q}^{-1} \mathbf{H}_2$ in step (a), whereas steps (b) and (c) follow from the properties of the Frobenius norm and the vectorization operator, respectively. While the alternative form in (12) for (11)'s objective function does not transform (11) to a convex optimization problem, replacing (12) in (11) lends the resulting problem to

being handled by the following two proposed efficient approaches: *i*) the gradient-based one; and *ii*) the MM approach.

1) *Gradient Descent Approach*: The optimization problem $\min_{\Theta} \mathcal{F}(\Phi(\Theta))$ using (12) is an unconstrained problem, hence, we can employ gradient search to monotonically decrease its objective, eventually converging to a stationary point. To begin with, we first define the matrices:

$$\mathbf{A} \triangleq (\overline{\mathbf{H}}_2^{+H} \otimes \mathbf{H}_1^+)^H (\overline{\mathbf{H}}_2^{+H} \otimes \mathbf{H}_1^+) \in \mathbb{C}^{N^2 \times N^2}, \quad (13)$$

$$\mathbf{y} \triangleq \text{vec}(\Phi^{-1}(\Theta)) \in \mathbb{C}^{N^2 \times 1}, \quad (14)$$

which help us to express (12) as $\mathcal{F}(\Phi(\Theta)) = \mathbf{y}^H \mathbf{A} \mathbf{y}$. To compute the gradient of $\mathcal{F}(\Phi(\Theta))$ with respect to Θ , i.e., $\nabla_{\Theta}(\mathbf{y}^H \mathbf{A} \mathbf{y})$, we expand $\mathbf{y}^H \mathbf{A} \mathbf{y}$ using (14) and the definition $\Phi(\Theta) = \text{diag}[e^{j\theta_1}, e^{j\theta_2}, \dots, e^{j\theta_N}]$ as

$$\mathbf{y}^H \mathbf{A} \mathbf{y} = \sum_{n=1}^N \sum_{m=1}^N a_{mn} e^{j(\theta_n - \theta_m)}, \quad (15)$$

where a_{mn} with $m, n = 1, 2, \dots, N$ denotes the (m, n) -th element of \mathbf{A} .

Then, the derivative of $\mathbf{y}^H \mathbf{A} \mathbf{y}$ with respect to $\theta_i \forall i = 1, 2, \dots, N$ can be computed as

$$\frac{\partial(\mathbf{y}^H \mathbf{A} \mathbf{y})}{\partial \theta_i} = j \phi_i^{-1} \sum_{m=1}^{N^2} a_{mi} (\phi_m^{-1})^* - j (\phi_i^{-1})^* \sum_{n=1}^{N^2} a_{in} \phi_n^{-1}. \quad (16)$$

However, since $\mathbf{A} = \mathbf{A}^H$, it holds that $a_{mi} = (a_{im}^*)$. Using the latter expression, (16) can be simplified to

$$\frac{\partial(\mathbf{y}^H \mathbf{A} \mathbf{y})}{\partial \theta_i} = 2\text{Re} \left(-j (\phi_n^{-1})^* \sum_{n=1}^{N^2} a_{in} \phi_n^{-1} \right), \quad (17)$$

which leads to the following expression for the desired gradient:

$$\nabla_{\Theta}(\mathbf{y}^H \mathbf{A} \mathbf{y}) = 2\text{Re}(-j \mathbf{y}^* \circ (\mathbf{A} \mathbf{y})). \quad (18)$$

To proceed with this approach, a suitable step size for the gradient descent needs to be computed. To this end, denote by $\text{vec}(\Theta)^t$ the phase of \mathbf{y} at iteration t , and by \mathbf{d}^t the adopted descent direction at iteration t . Then, the next iteration point is given by

$$\text{vec}(\Theta)^{(t+1)} = \text{vec}(\Theta)^{(t)} + \mu \mathbf{d}^{(t)}, \quad (19)$$

$$\mathbf{y}^{(t+1)} = e^{j \text{vec}(\Theta)^{(t+1)}} \circ \text{vec}(\mathbf{I}_N) = \mathbf{y}^{(t)} \circ e^{j \mu \mathbf{d}^{(t)}} \circ \text{vec}(\mathbf{I}_N), \quad (20)$$

where $\mu > 0$ is the step size. In order to find a suitable step size, we need to solve the following minimization problem:

$$\min_{\mu > 0} h(\mu) \triangleq (\mathbf{y}^{(t+1)})^H \mathbf{A} \mathbf{y}^{(t+1)}, \quad (21)$$

To do so, we expand $h(\mu)$ as follows:

$$(\mathbf{y}^{(t+1)})^H \mathbf{A} \mathbf{y}^{(t+1)} = \sum_{m,n=1}^{N^2} a_{mn=1} ((\phi_m^{-1})^*)^{(t)} (\phi_n^{-1})^{(t)} e^{j\mu(d_n^{(t)} - d_m^{(t)})}, \quad (22)$$

where $(\phi_n^{-1})^{(t)}$ and $d_n^{(t)}$ are respectively the n -th elements of $\mathbf{x}^{(t)}$ and $\mathbf{d}^{(t)}$. To obtain a more tractable expression than (22), we simplify by considering the second-order Taylor expansion of the term $e^{j\mu(d_n^{(t)} - d_m^{(t)})}$ around $\mu = 0$, namely

$$e^{j\mu(d_n^{(t)} - d_m^{(t)})} \approx 1 + j\mu(d_n^{(t)} - d_m^{(t)}) + \frac{(j\mu(d_n^{(t)} - d_m^{(t)}))^2}{2!}. \quad (23)$$

By substituting (23) into (22), the following approximation for $h(\mu)$ can be derived

$$\begin{aligned} (\mathbf{y}^{(t+1)})^H \mathbf{A} \mathbf{y}^{(t+1)} &\approx \sum_{m,n=1}^{N^2} a_{mn=1} ((\phi_m^{-1})^*)^{(t)} (\phi_n^{-1})^{(t)} \left(1 + j\mu(d_n^{(t)} - d_m^{(t)}) + \frac{(j\mu(d_n^{(t)} - d_m^{(t)}))^2}{2!} \right) \\ &= (\mathbf{y}^{(t)})^H \mathbf{A} \mathbf{y}^{(t)} + j\mu \left((\mathbf{y}^{(t)})^H \mathbf{A} \mathbf{y}_1^{(t)} - (\mathbf{y}_1^{(t)})^H \mathbf{A} \mathbf{y}^{(t)} \right) - \frac{\mu^2}{2} \left((\mathbf{y}^{(t)})^H \mathbf{A} \mathbf{y}_2^{(t)} \right. \\ &\quad \left. - (\mathbf{y}_2^{(t)})^H \mathbf{A} \mathbf{y}^{(t)} - 2(\mathbf{y}_1^{(t)})^H \mathbf{A} \mathbf{y}_1^{(t)} \right) \\ &= (\mathbf{y}^{(t)})^H \mathbf{A} \mathbf{y}_1^{(t)} - 2\mu \text{Im} \left((\mathbf{y}^{(t)})^H \mathbf{A} \mathbf{y}_1^{(t)} \right) + \mu^2 \left((\mathbf{y}_1^{(t)})^H \mathbf{A} \mathbf{y}_1^{(t)} \right) \\ &\quad - \mu^2 \left(\text{Re} \left((\mathbf{y}^{(t)})^H \mathbf{A} \mathbf{y}_2^{(t)} \right) \right), \end{aligned} \quad (24)$$

where $\mathbf{y}_1^{(t)} = \mathbf{y}^{(t)} \circ \mathbf{d}^{(t)}$ and $\mathbf{y}_2^{(t)} = \mathbf{y}^{(t)} \circ \mathbf{d}^{(t)} \circ \mathbf{d}^{(t)}$. We finally use the definition $z_1 \triangleq (\mathbf{y}^{(t)})^H \mathbf{A} \mathbf{y}^{(t)}$, $z_2 \triangleq \text{Im} \left((\mathbf{y}^{(t)})^H \mathbf{A} \mathbf{y}_1^{(t)} \right)$, and $z_3 \triangleq \text{Re} \left((\mathbf{y}^{(t)})^H \mathbf{A} \mathbf{y}_2^{(t)} \right) - (\mathbf{y}_1^{(t)})^H \mathbf{A} \mathbf{y}_1^{(t)}$ to express the latter approximation for $h(\mu)$ in the compact form

$$\widehat{h}(\mu) = z_1 - 2z_2\mu - z_3\mu^2. \quad (25)$$

By virtue of (21) and (25), it follows that $h(0) = \widehat{h}(0) = z_1$, which indicates that the quartic function $\widehat{h}(\mu)$ passes through the point $(0, z_1)$. Setting the first-order derivative of $\widehat{h}(\mu)$ to zero yields the minimum step size as:

$$\mu = -\frac{z_2}{z_3}. \quad (26)$$

Equipped with the expression (18) for the gradient of our objective function $\mathcal{F}(\Phi(\Theta))$ given by (12), as well as the expression (26) for the step size, we can employ the Polak-Ribiere-Polyok conjugate gradient algorithm [41], [42] to update the descent direction using the following formula:

$$\mathbf{d}^{(t+1)} = -\mathbf{q}^{(t+1)} + \frac{(\mathbf{q}^{(t+1)} - \mathbf{q}^{(t)})^T \mathbf{q}^{(t+1)}}{\|\mathbf{q}^{(t)}\|^2} \mathbf{d}^{(t)}, \quad (27)$$

where $\mathbf{q}^{(t)} \triangleq \nabla_{\Theta} ((\mathbf{y}^{(t)})^H \mathbf{A} \mathbf{y}^{(t)})$. However, since the step size is an approximate value, $(\mathbf{q}^{(t+1)})^T \mathbf{d}^{(t)}$ is not equal to zero. Thus, $\mathbf{d}^{(t)}$ may not be descent, i.e., the following property

$$(\mathbf{q}^{(t+1)})^T \mathbf{d}^{(t+1)} = -\|\mathbf{q}^{(t+1)}\|^2 + \frac{(\mathbf{q}^{(t+1)} - \mathbf{q}^{(t)})^T \mathbf{q}^{(t+1)}}{\|\mathbf{q}^{(t)}\|^2} (\mathbf{q}^{(t+1)})^T \mathbf{d}^{(t)} < 0 \quad (28)$$

might not be always satisfied. To guarantee that the search direction is always a descent direction, we apply the following modified direction:

$$\mathbf{d}^{(t+1)} = \begin{cases} \mathbf{d}^{(t+1)}, & (\mathbf{q}^{(t+1)})^T \mathbf{d}^{(t+1)} < 0 \\ -\mathbf{q}^{(t+1)}, & (\mathbf{q}^{(t+1)})^T \mathbf{d}^{(t+1)} \geq 0 \end{cases}.$$

2) *Majorization-Minimization (MM) Approach:* By substituting (12) into (10), the optimization problem with respect to Φ for given \mathbf{P} can be rewritten as

$$\min_{\Phi} \text{vec}(\Phi^{-1})^H \mathbf{A} \text{vec}(\Phi^{-1}) \quad (29a)$$

$$\text{s.t. } |\phi_n| = 1 \quad \forall n = 1, 2, \dots, N, \quad (29b)$$

As it will be shown in the sequel, the form of the objective in (29a) enables us to deal with the non-convex constraint (29b), provided that (29a) can be reformulated into a differentiable function. To this end, a convenient approach is to resort to the MM method, also known as sequential optimization method or inner approximation method [10], [43]–[46].

The basic idea of the MM method is to tackle a difficult problem by solving a sequence of approximate subproblems. If each approximate problem fulfills some assumptions with respect to the original problem, then the sequence converges and first-order optimality holds upon convergence. In more detail, consider the following general optimization program:

$$\min_{\mathbf{x}} \bar{f}(\mathbf{x}) \quad (30a)$$

$$\text{s.t. } g_i(\mathbf{x}) \leq 0 \quad \forall i = 1, 2, \dots, I. \quad (30b)$$

Consider also the sequence $\{\mathbf{x}^{(t)}\}$ of feasible points for (30), and the the sequence of minimization problems $\mathcal{P}_{\mathbf{x}^{(t)}}$ with objectives $f(\mathbf{x}|\mathbf{x}^{(t)})$ and the same constraints as (30). If for each $\mathbf{x}^{(t)}$ the following conditions are fulfilled:

- 1) $f(\mathbf{x}|\mathbf{x}^{(t)}) \geq \bar{f}(\mathbf{x})$ for all feasible \mathbf{x} ,
- 2) $f(\mathbf{x}^{(t)}|\mathbf{x}^{(t)}) = \bar{f}(\mathbf{x}^{(t)})$,
- 3) $\nabla_{\mathbf{x}}f(\mathbf{x}^{(t)}|\mathbf{x}^{(t)}) = \nabla_{\mathbf{x}}\bar{f}(\mathbf{x}^{(t)})$,

then the optimal sequence $\{(\mathbf{x}^*)^{(t)}\}$ of the solutions for the problems $\mathcal{P}_{\mathbf{x}^{(t)}}$ monotonically decreases the original objective function value $\bar{f}(\mathbf{x}^{(t)})$, and it thus converges. Moreover, upon convergence, the first-order optimality properties of problem (30) are satisfied [10], [43]–[46]. Clearly, the usefulness of the MM method depends on the possibility of determining suitable functions $f(\mathbf{x}|\mathbf{x}^{(t)})$ meeting the above three conditions. In addition, these functions need to be easier than (29a) to minimize.

For the optimization problem (29) at hand, the MM method can be applied as described in the rest of this section. We commence with the following lemma that provides a convenient upper bound for the objective $\mathbf{y}^H \mathbf{A} \mathbf{y}$ in (29a) (the definition $\mathbf{y} = \text{vec}(\Phi^{-1})$ in (14) is reused).

Lemma 1: For any feasible \mathbf{y} for (29), and given any feasible point $\mathbf{y}^{(t)}$, a suitable upper bound to employ the MM method is:

$$\mathbf{y}^H \mathbf{A} \mathbf{y} \leq f(\mathbf{y}|\mathbf{y}^{(t)}) = \mathbf{y}^H \mathbf{M} \mathbf{y} - 2\text{Re}(\mathbf{y}^H (\mathbf{M} - \mathbf{A}) \mathbf{y}^{(t)}) + (\mathbf{y}^{(t)})^H (\mathbf{M} - \mathbf{A}) \mathbf{y}^{(t)}, \quad (31)$$

where $\mathbf{M} \triangleq \lambda_{\max} \mathbf{I}_{N^2}$ with λ_{\max} being the maximum eigenvalue of \mathbf{A} .

Proof: Let us consider the following inequality:

$$\|(\mathbf{M} - \mathbf{A})^{1/2} \mathbf{y} - (\mathbf{M} - \mathbf{A})^{1/2} \mathbf{y}^{(t)}\|^2 \geq 0. \quad (32)$$

Since the matrix $\mathbf{M} - \mathbf{A}$ is positive semidefinite by construction, elaborating the latter inequality yields

$$\mathbf{y}^H (\mathbf{M} - \mathbf{A}) \mathbf{y} + (\mathbf{y}^{(t)})^H (\mathbf{M} - \mathbf{A}) \mathbf{y}^{(t)} - 2\text{Re}(\mathbf{y}^H (\mathbf{M} - \mathbf{A}) \mathbf{y}^{(t)}) \geq 0. \quad (33)$$

By isolating the term $\mathbf{y}^H \mathbf{A} \mathbf{x}$, we obtain the bound in (31); this completes the proof. \blacksquare

Lemma 1 provides a suitable expression for the surrogate function in terms of the variable \mathbf{y} to be used with the MM method. The next step is to reformulate constraint (29b) also in terms of the variable \mathbf{y} . Here, it should be paid attention to the fact that (29b) enforces the diagonal elements of Φ to have unit modulus, whereas \mathbf{y} contains the elements of the vectorized Φ . Thus, only some elements of \mathbf{y} need to have unit modulus, while all others are bound to

be zero. More precisely, the \mathbf{y} 's elements that must have unit modulus are those with indices of the form $(i-1)N + i$, with $i = 1, 2, \dots, N$. For example, if $N = 5$, we have the indices $\{1, N+2, 2N+3, 3N+4, 4N+5 = N^2 = 25\}$.

Putting all above together, each iteration of the MM method requires solving the following problem with respect to the variable \mathbf{y} (from which the optimal Φ can be easily obtained):

$$\min_{\mathbf{y}} f(\mathbf{y}|\mathbf{y}^{(t)}) \quad (34a)$$

$$\text{s.t. } |y_i| = 1, \forall i = (n-1)N + n, n = 1, 2, \dots, N, \quad (34b)$$

$$y_i = 0, \forall i \neq (n-1)N + n, n = 1, 2, \dots, N, \quad (34c)$$

where y_n denotes the n -element of vector \mathbf{y} . In the following lemma we present the solution for (34).

Lemma 2: For any $\mathbf{y}^{(t)}$, the optimization problem (34) is solved by

$$y_i = \begin{cases} e^{j\arg(c_i)}, \forall i = (n-1)N + n, n = 1, 2, \dots, N \\ 0, \quad \forall i \neq (n-1)N + n, n = 1, 2, \dots, N \end{cases}, \quad (35)$$

where c_m 's with $m = 1, 2, \dots, N^2$ are the elements of $\mathbf{c} \triangleq (\lambda_{\max}\mathbf{I}_{N^2} - \mathbf{A})\mathbf{y}^{(t)}$.

Proof: The objective function (34a) can be expressed as

$$f(\mathbf{y}|\mathbf{y}^{(t)}) = \lambda_{\max}\|\mathbf{y}\|^2 - 2\text{Re}(\mathbf{y}^H(\lambda_{\max}\mathbf{I}_{N^2} - \mathbf{A})\mathbf{y}^{(t)}) + (\mathbf{y}^{(t)})^H(\lambda_{\max}\mathbf{I}_{N^2} - \mathbf{A})\mathbf{y}^{(t)}. \quad (36)$$

By neglecting the terms that do not depend on \mathbf{y} and observing that by virtue of (34b) and (34c) it holds $\|\mathbf{y}\|^2 = N^2$, problem (34) can be equivalently recast as

$$\max_{\mathbf{y}} 2\text{Re}(\mathbf{y}^H(\lambda_{\max}\mathbf{I}_{N^2} - \mathbf{A})\mathbf{y}^{(t)}) \quad (37a)$$

$$\text{s.t. } |y_i| = 1, \forall i = (n-1)N + n, n = 1, 2, \dots, N, \quad (37b)$$

$$y_i = 0, \forall i \neq (n-1)N + n, n = 1, 2, \dots, N. \quad (37c)$$

Clearly, the only free variables are the phases of the y_i 's components whose modulus is constrained to be unity, whereas all other components of \mathbf{y} are constrained to be zero. Then, (37a) can be seen to be maximized when the phases of the non-zero components of y_i 's are aligned with those of the corresponding components of the vector $(\lambda_{\max}\mathbf{I}_{N^2} - \mathbf{A})\mathbf{y}^{(t)}$. Hence, (35) is obtained. ■

Algorithm 1 Dinkelbach's Method

- 1: **Initialization:** $K, b, \xi, P_{\text{BS}}, P_{\text{UE}}, P_n(b), \epsilon > 0$, and $\lambda_0 = 0$.
 - 2: **for** $i = 1, 2, \dots$ **do**
 - 3: Solve the concave maximization:

$$\mathbf{P}_i^* = \arg \max_{\mathbf{P} \in \mathcal{B}} \sum_{k=1}^K \log_2(1 + p_k \sigma^{-2}) - \lambda_{i-1} (\xi \sum_{k=1}^K p_k + P_{\text{BS}} + K P_{\text{UE}} + N P_n(b)).$$
 - 4: Set $\lambda_i = \frac{\sum_{k=1}^K \log_2(1 + p_{k,i}^* \sigma^{-2})}{\xi \sum_{k=1}^K p_{k,i}^* + P_{\text{BS}} + K P_{\text{UE}} + N P_n(b)}$.
 - 5: **if** $|\lambda_i - \lambda_{i-1}| < \epsilon$ **then**
 - 6: **Output:** \mathbf{P}_i^* .
 - 7: **end if**
 - 8: **end for**
-

B. Optimization with respect to the Power Allocation \mathbf{P}

We now turn again our attention in problem (8) for the case where Φ is fixed and the objective is the optimization over \mathbf{P} . Particularly, we focus on solving:

$$\max_{\mathbf{P}} \frac{\sum_{k=1}^K \log_2(1 + p_k \sigma^{-2})}{\sum_{k=1}^K \mu_k p_k + P_{\text{BS}} + K P_{\text{UE}} + N P_n(b)} \quad (38a)$$

$$\text{s.t. } p_k \geq \sigma^2(2^{R_{\min,k}} - 1), \quad \forall k = 1, 2, \dots, K, \quad (38b)$$

$$\text{tr}((\mathbf{H}_2 \Phi \mathbf{H}_1)^+ \mathbf{P} (\mathbf{H}_2 \Phi \mathbf{H}_1)^{+H}) \leq P_{\max}. \quad (38c)$$

It is can be that, for fixed Φ , the numerator of (38a) is concave in \mathbf{P} , while the denominator of (38a) is convex in \mathbf{P} . Moreover, both constraints (38b) and (38c) are also convex with respect to \mathbf{P} . As a consequence, problem (38) is a single-ratio maximization problem that can be globally solved with limited complexity using Dinkelbach's algorithm [10]. This method is summarized in Algorithm 1, where set $\mathcal{B} \triangleq \{\mathbf{P} = \text{diag}[p_1, p_2, \dots, p_K] : (38b) \wedge (38c)\}$ and $\mathbf{P}_i^* \triangleq \text{diag}[p_{1,i}^*, p_{2,i}^*, \dots, p_{K,i}^*]$ denotes the transmit power allocation solution in Step 3 at each i -th (with $i = 1, 2, \dots$) algorithmic iteration.

Putting together the solutions for Φ and \mathbf{P} presented respectively in Sections III-A and III-B, our two proposed EE maximization algorithms for the considered LIS-assisted multi-user MISO system are summarized in Algorithms 2 and 3. As shown, the solutions for Φ and \mathbf{P} are alternatively and iteratively deployed till reaching convergence of their solutions between consecutive runs (particularly, the squared norm of their difference) that is smaller than a small $\epsilon > 0$. In both algorithms, subscript ℓ (with $\ell = 1, 2, \dots$) in Φ and \mathbf{P} indicates their values at the ℓ -th

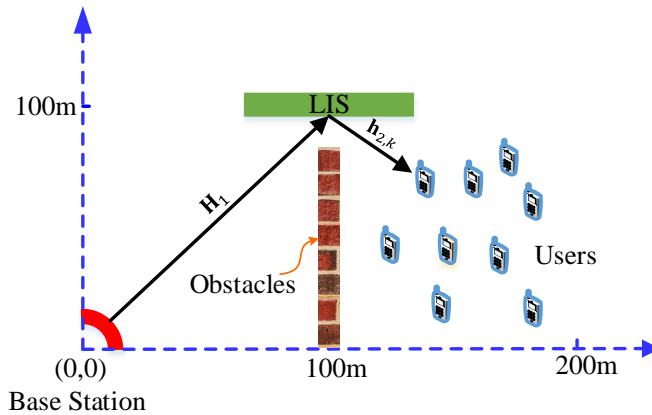


Figure 2. The simulated LIS-assisted K -user MISO communication scenario comprising of a M -antenna base station and a N -element intelligent surface.

algorithmic iteration. Note that, at each iteration, both approaches increase the EE value, thus converging in the value of the objective. This happens because the objective is continuous over the compact feasible set of (8), and thus is upper-bounded [41], [42], [47]–[51]. However, no global optimality claim can be made due to the following facts: *i*) problem (8) is not jointly convex with respect to both \mathbf{P} and Φ ; and *ii*) the proposed methods for optimizing Φ (when \mathbf{P} is fixed) are not guaranteed to yield the globally optimal phase matrix.

C. Sum Rate Maximization

In the previous Section III we focused on the EE maximization problem (8). It should be stressed, however, that is a special case of the EE maximization problem of the considered LIS-assisted system. More specifically, it can be seen from (8) that the system sum rate performance is given by the numerator in (8a). Hence, Algorithm 2 can be specialized to the sum rate maximization by simply setting $\xi = 0$. By doing this, the denominator of (8a) reduces to a constant, and maximizing (8a) reduces to the maximization of the sum rate. In particular, this modification affects the optimization with respect to the transmit powers, which reduces to a non-fractional and convex problem that can be solved by a single iteration of Algorithm 1.

IV. NUMERICAL RESULTS

In this section, we investigate the performance of the LIS-assisted K -user MISO communication system illustrated in Fig. 2. The multiple single-antenna mobile users are assumed randomly and uniformly placed in the $100m \times 100m$ half right-hand side rectangular of the figure. All

Algorithm 2 Gradient-based EE Maximization Algorithm

- 1: **Input:** $K, b, \xi, P_{BS}, P_{UE}, P_n(b), P_{\max}, \sigma^2, \{R_{\min,k}\}_{k=1}^K, \mathbf{H}_2, \mathbf{H}_1,$ and $\epsilon > 0.$
 - 2: **Initialization:** $\mathbf{P}^0 = \frac{P_{\max}}{K} \mathbf{I}_K, \Phi^0 = \frac{\pi}{2} \mathbf{I}_N, \mathbf{q}^0 = \nabla_{\Theta}((\mathbf{y}^0)^H \mathbf{A} \mathbf{y}^0),$ and $\mathbf{d}^0 = -\mathbf{q}^0.$
 - 3: **for** $\ell = 0, 1, 2, \dots$ **do**
 Given \mathbf{P} update Φ :
 4: **for** $t = 0, 1, 2, \dots$ **do**
 5: $\mathbf{y}_1^{(t)} = \mathbf{y}^{(t)} \circ \mathbf{d}^{(t)}.$
 6: $\mathbf{y}_2^{(t)} = \mathbf{y}^{(t)} \circ \mathbf{d}^{(t)} \circ \mathbf{d}^{(t)}.$
 7: $z_2 = \text{Im}((\mathbf{y}^{(t)})^H \mathbf{A} \mathbf{y}_1^{(t)}),$
 8: $z_3 = \text{Re}((\mathbf{y}^{(t)})^H \mathbf{A} \mathbf{y}_2^{(t)}) - (\mathbf{y}_1^{(t)})^H \mathbf{A} \mathbf{y}_1^{(t)}.$
 9: Compute $\hat{h}(\mu) = 0$ using (25).
 10: Set the step size as $\mu = -\frac{z_2}{z_3}.$
 11: $\mathbf{y}^{(t+1)} = \mathbf{y}^{(t)} \circ e^{j\mu \mathbf{d}^{(t)}} \circ \text{vec}(\mathbf{I}_N).$
 12: $\mathbf{q}^{(t+1)} = 2\text{Re}(-j(\mathbf{y}^*)^{(t+1)} \circ (\mathbf{A} \mathbf{y}^{(t+1)})).$
 13: $\mathbf{d}^{(t+1)} = -\mathbf{q}^{(t+1)} + \frac{(\mathbf{q}^{(t+1)} - \mathbf{q}^{(t)})^T \mathbf{q}^{(t+1)}}{\|\mathbf{q}^{(t)}\|^2} \mathbf{d}^{(t)}.$
 14: $\mathbf{d}^{(t+1)} = \begin{cases} \mathbf{d}^{(t+1)}, & (\mathbf{q}^{(t+1)})^T \mathbf{d}^{(t+1)} < 0 \\ -\mathbf{q}^{(t+1)}, & (\mathbf{q}^{(t+1)})^T \mathbf{d}^{(t+1)} \geq 0 \end{cases}.$
 15: **Until** $\|\Phi^{(t+1)} - \Phi^{(t)}\|^2 < \epsilon;$ Obtain $\Phi^{(\ell+1)} = \Phi^{(t+1)}.$
 16: **end for**
 Given Φ update \mathbf{P} :
 17: **if** (10a) evaluated at $\Phi^{(\ell+1)}$ is lower than P_{\max} **then:**
 18: Update \mathbf{P} by solving the following problem using Algorithm 1:
 19: $\mathbf{P}^{(\ell+1)} = \arg \max_{\mathbf{P} \in \mathcal{B}} \frac{\sum_{k=1}^K \log_2(1 + p_k \sigma^{-2})}{\xi \sum_{k=1}^K p_k + P_{BS} + K P_{UE} + N P_n(b)}$
 20: **elseBreak** and declare infeasibility.
 21: **end if**
 22: **Until** $\|\Phi^{(\ell+1)} - \Phi^{(\ell)}\|^2 < \epsilon$ and $\|\mathbf{P}^{(\ell+1)} - \mathbf{P}^{(\ell)}\|^2 < \epsilon.$
 23: **Output:** $\Phi^{(\ell+1)}$ and $\mathbf{P}^{(\ell+1)}.$
 24: **end for**
-

presented illustrations include average results over 10^3 independent realizations of the users' positions and channel realizations. For the latter realizations we have used the 3GPP propagation

Algorithm 3 MM-based EE Maximization Algorithm

- 1: **Input:** $K, b, \xi, P_{\text{BS}}, P_{\text{UE}}, P_n(b), P_{\text{max}}, \sigma^2, \{R_{\min,k}\}_{k=1}^K, \mathbf{H}_2, \mathbf{H}_1,$ and $\epsilon > 0.$
 - 2: **Initialization:** $\mathbf{P}^0 = \frac{P_{\text{max}}}{K} \mathbf{I}_K$ and $\Phi^0 = \frac{\pi}{2} \mathbf{I}_N.$
 - 3: **for** $\ell = 0, 1, 2, \dots$ **do**
 Optimize with respect to Φ given \mathbf{P} :
 - 4: **for** $t = 0, 1, 2, \dots$ **do**
 - 5: $\mathbf{A} = (\overline{\mathbf{H}}_2^{+H} \otimes \mathbf{H}_1^+)^H (\overline{\mathbf{H}}_2^{+H} \otimes \mathbf{H}_1^+).$
 - 6: $\mathbf{y} \triangleq \text{vec}(\Phi^{-1}).$
 - 7: Compute \mathbf{y} as in (35).
 - 8: $\mathbf{y}^{(t+1)} = \text{reshape}(\mathbf{y});$
 - 9: **Until** $\|\Phi^{(t+1)} - \Phi^{(t)}\|^2 < \epsilon,$
 - 10: Obtain $\Phi^{(\ell+1)} = \Phi^{(t+1)};$
 - 11: **end for**
 Optimize with respect to \mathbf{P} given Φ :
 - 12: **if** (10a) evaluated at $\Phi^{(\ell+1)}$ is lower than P_{max} **then:**
 - 13: Update \mathbf{P} by solving the following problem using Algorithm 1:
 - 14:
$$\mathbf{P}^{(\ell+1)} = \arg \max_{\mathbf{P} \in \mathcal{B}} \frac{\sum_{k=1}^K \log_2(1+p_k \sigma^{-2})}{\xi \sum_{k=1}^K p_k + P_{\text{BS}} + K P_{\text{UE}} + N P_n(b)}$$
 - 15: **else** Break and declare infeasibility.
 - 16: **end if**
 - 17: **Until** $\|\Phi^{(\ell+1)} - \Phi^{(\ell)}\|^2 < \epsilon$ and $\|\mathbf{P}^{(\ell+1)} - \mathbf{P}^{(\ell)}\|^2 < \epsilon.$
 - 18: **Output:** $\Phi^{(\ell+1)}$ and $\mathbf{P}^{(\ell+1)}.$
 - 19: **end for**
-

environment described in [52], whose parameters are summarized in Table I. Therein, notations $[\mathbf{H}_1]_{ij}$ and $[\mathbf{h}_{2,k}]_i$ with $i = 1, 2, \dots, N$, $k = 1, 2, \dots, K$, and $j = 1, 2, \dots, M$ represent the (i, j) -th and i -th elements of the respective matrices. In this table, we also include the hardware dissipation parameters of [10], [16] for BS, LIS, and the mobile users, as well as for the AF relay that will be used for performance comparisons purposes. The relay is assumed to transmit with maximum power $P_{\text{R,max}}$, which is considered in all performance results equal to P_{max} .

Without loss of generality, in the figures that follow we assume equal individual rate constraints for all K users, i.e., $R_{\min,k} = R_{\min} \forall k$. In addition, we set R_{\min} to a fraction of the rate that

Table I
SIMULATION AND ALGORITHMIC PARAMETERS

Parameters	Values
LIS central element placement:	$(100m, 100m)$
BS central element placement:	$(0, 0)$
Small scale fading model $\forall i, k, j$:	$[\mathbf{H}_1]_{ij}, [\mathbf{h}_{2,k}]_i \sim \mathcal{CN}(0, 1)$
Large scale fading model at distance d :	$\frac{10^{-3.53}}{d^{3.76}}$
Transmission bandwidth BW:	180kHz
Circuit dissipated power at BS P_{BS} :	100dBm
Circuit dissipated power coefficients at BS ξ and AF relay ξ_{AF} :	1.2
Maximum transmit power at BS and AF relay $P_{\max}=P_{R,\max}$:	20dBW
Dissipated power at each user P_{UE} :	10dBm
Dissipated power at the n -th LIS element $P_n(b)$:	10dBm
Dissipated power at each AF relay transmit-receive antenna P_R :	10dBm
Algorithmic convergence parameter:	$\epsilon > 10^{-3}$

each user would have in the genie case of mutually orthogonal channels and uniform power allocation. In particular, this genie rate for each k -th mobile user is given by

$$R = \log_2 \left(1 + \frac{P_{\max}}{K\sigma^2} \right). \quad (39)$$

Note that setting $R_{\min} = R$ in our EE maximization formulation would lead to an unfeasible problem, hence, it should hold $R_{\min} < R$.

A. Benchmark: Amplify-and-Forward (AF) Relay

It is reasonable to expect that the consideration of a reconfigurable LIS structure in the investigated scenario of Fig. 2 provides substantial EE gains compared to the case where such a surface is absent; this intuition has been verified via simulations in [1]. Hereinafter, we consider a more relevant to Fig. 2 benchmark scheme that includes a conventional N -antenna AF relay [22]–[25] in the place of the LIS structure. To ensure a fair comparison between this benchmark scheme and our proposed LIS-assisted one in the performance results that follow, we have considered the same users' positions and channel realizations in both cases. Similar to the LIS case modeled by the phase shifting matrix Φ , we assume that the relay deploys the $N \times N$ complex diagonal AF matrix \mathbf{V} . Differently from Φ , \mathbf{V} 's diagonal elements are not constrained to have unit modulus, but rather a maximum relay power constraint is enforced. In more detail,

the baseband received signals $\mathbf{y}_R \in \mathbb{C}^{N \times 1}$ and $\mathbf{y}_K \in \mathbb{C}^{K \times 1}$ at the relay and at all K mobile users, respectively, can be expressed as

$$\mathbf{y}_R \triangleq \mathbf{H}_1 \mathbf{x} + \mathbf{w}_R, \quad (40)$$

$$\mathbf{y}_K \triangleq \mathbf{H}_2 \mathbf{V} \mathbf{y}_R + \mathbf{w}_K = \mathbf{H}_2 \mathbf{V} \mathbf{H}_1 \mathbf{x} + \mathbf{H}_2 \mathbf{V} \mathbf{w}_r + \mathbf{w}_K, \quad (41)$$

where $\mathbf{w}_R \in \mathbb{C}^{N \times 1}$ denote the thermal noise at relay modeled as a zero-mean complex circularly Gaussian vector with covariance matrix \mathbf{I}_N . We model similarly the thermal noises at all K users, which are included in $\mathbf{w}_K \in \mathbb{C}^{K \times 1}$ having covariance matrix \mathbf{I}_K .

It is interesting to observe that, since the AF matrix \mathbf{V} is not unitary, it introduces a noise amplification effect that is not present in the LIS case. Moreover, as already anticipated, unlike LIS, the AF relay consumes RF power to amplify the incoming signal. Accounting for ZF transmission from BS as in the LIS design case in (8), the relay power consumption is given by

$$P_{\text{AF}} \triangleq \text{tr}(\mathbf{H}_2^+ \mathbf{P} \mathbf{H}_2^{+H} + \mathbf{V} \mathbf{V}^H \sigma^2). \quad (42)$$

Hence, for the case of AF relaying, we consider the following EE maximization problem for the joint design of \mathbf{P} and \mathbf{V} :

$$\max_{\mathbf{V}, \mathbf{P}} \frac{\sum_{k=1}^K \log_2 \left(1 + \frac{p_k}{|\mathbf{h}_{2,k} \mathbf{V} \mathbf{V}^H \mathbf{h}_{2,k}^H|^2 + \sigma^2} \right)}{\xi \sum_{k=1}^K p_k + P_{\text{BS}} + K P_{\text{UE}} + \xi_{\text{AF}} P_{\text{AF}} + N P_{\text{R}}} \quad (43a)$$

$$\text{s.t. } \log_2 \left(1 + \frac{p_k}{|\mathbf{h}_{2,k} \mathbf{V} \mathbf{V}^H \mathbf{h}_{2,k}^H|^2 + \sigma^2} \right) \geq R_{\min,k} \quad \forall k = 1, 2, \dots, K, \quad (43b)$$

$$\text{tr}((\mathbf{H}_2 \mathbf{V} \mathbf{H}_1)^+ \mathbf{P} (\mathbf{H}_2 \mathbf{V} \mathbf{H}_1)^{+H}) \leq P_{\max}, \quad (43c)$$

$$\text{tr}(\mathbf{H}_2^+ \mathbf{P} \mathbf{H}_2^{+H} + \mathbf{V} \mathbf{V}^H \sigma^2) \leq P_{\text{R,max}}, \quad (43d)$$

where ξ_{AF} depends on the efficiency of the relay power amplifier. In order to solve (43) we resort again to the alternating optimization method, like in the LIS case. The optimization with respect to \mathbf{P} for a given \mathbf{V} can be performed following a similar approach to Section III-B, whereas the optimization with respect to \mathbf{V} for a given \mathbf{P} becomes more challenging due to the presence of constraint (43c). To find the optimum \mathbf{V} in the results that follow we have employed numerical exhaustive search.

B. LIS vs AF relay Performance Comparison

The achievable sum rate and EE performances as functions of P_{\max} in dBm are illustrated in Figs. 3 and 4, respectively. We have evaluated the gradient- and MM-based approaches described

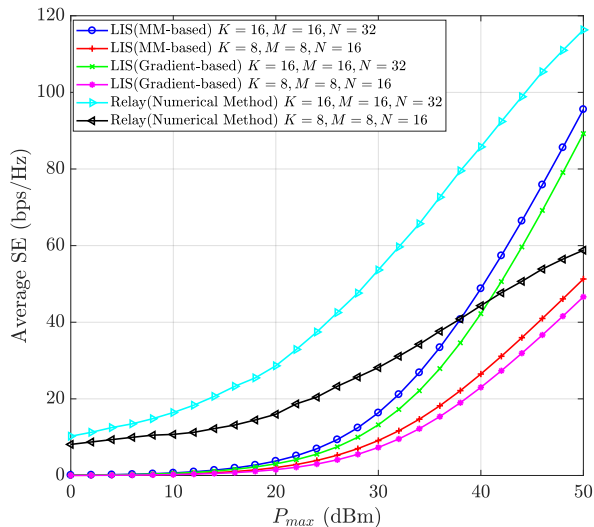


Figure 3. Average sum rate using either LIS or AF relay versus P_{\max} for $R_{\min} = 0$ bps/Hz and: a) $K = 16$, $M = 16$, $N = 32$; and b) $K = 8$, $M = 8$, $N = 16$.

in Algorithms 2 and 3, respectively, as well as the algorithm described in Section IV-A for the AF relay case. In both figures, we have set the minimum QoS constraint as $R_{\min} = 0$ bps/Hz for all K users, and considered the two different settings: a) $K = 16$, $M = 16$, and $N = 32$; and b) $K = 8$, $M = 8$, and $N = 16$. As seen from Fig. 3, the relay-assisted system outperforms the LIS-assisted one, irrespective of the proposed algorithm used. This behavior is expected since the AF relay is an active terminal rather than a reflecting structure as the LIS is. The relay possesses dedicated transmit circuitry that provides the transmit power $P_{R,\max}$ to it. Moreover, the relay is not constrained by the unit modulus constraint that the intelligent surface has. Specifically, LIS loses about 40bps/Hz and 20bps/Hz at $P_{\max} = 30$ dBm under the settings a) and b), respectively. However, as P_{\max} increases, the performance gap between the LIS and relay cases becomes smaller. This happens because as P_{\max} increases, the relay transmit power $P_{R,\max}$ becomes less and less relevant to the sum rate, which is actually impacted by the BS transmit power. It can be also observed from Fig. 3, which also holds in Figs. 4, that both proposed Algorithms 2 and 3 perform similarly, with the MM-based one achieving slightly better performance.

The trend in Fig. 3 is reversed in Fig. 4, where the EE performance is sketched. It is shown that both proposed algorithms for the LIS-assisted system case significantly outperform our derived algorithm for the relay-assisted one. Particularly, the EE of the LIS-assisted system is 300% larger than that of the one based on the AF relay when $P_{\max} \geq 32$ dBm. This is a direct

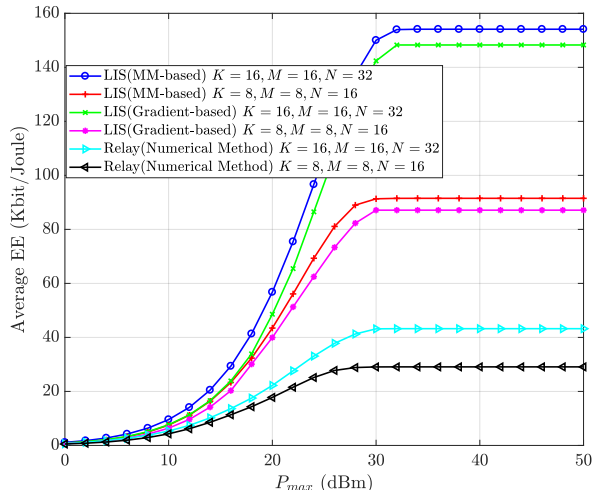


Figure 4. Average EE using either LIS or AF relay versus P_{\max} for $R_{\min} = 0\text{bps/Hz}$ and: a) $K = 16, M = 16, N = 32$; and b) $K = 8, M = 8, N = 16$.

consequence of the fact that former system exhibits a much lower energy consumption compared to the latter one. It is also shown that the setting a) with $K = 16, M = 16$, and $N = 32$ is more energy efficient than the setting b) with $K = 8, M = 8, N = 16$. It can be also observed that for both systems cases the EE performance saturates for $P_{\max} \geq 32\text{dBm}$. This explained by the fact that the EE function is not monotonically increasing with the maximum BS transmit power P_{\max} , but instead has a finite maximizer. When $P_{\max} \geq 32\text{dBm}$, the excess BS transmit power is actually not used since as it would only reduce the EE value.

C. Impact of the QoS Constraints

The effect of the different values for R_{\min} in the sum rate and EE performances versus P_{\max} in dBm is depicted in Figs. 5 and 6, respectively, using our MM-based algorithm 3. For the cases where the design problems turned out to be infeasible, the rate constraint has been removed and the unconstrained solutions were retained. Figure 5 shows that for low P_{\max} values the problem is nearly always infeasible. This is expected since there is not enough transmit power from BS to meet the rate requests of the users, and thus, the performance of all designed solutions coincide to very low sum rate values. However, for $P_{\max} \geq 16\text{dBm}$, the values for R_{\min} start having a significant impact on the sum rate. It can be observed that, increasing R_{\min} results in increasing the achievable sum rate and outperforming more the saturating unconstrained case of $R_{\min} = 0\text{bps/Hz}$. Obviously, the larger the R_{\min} value is, the higher the slope of the sum rate curve. The performance behavior in Fig. 6 follows the same trend with Fig. 5. We may see that

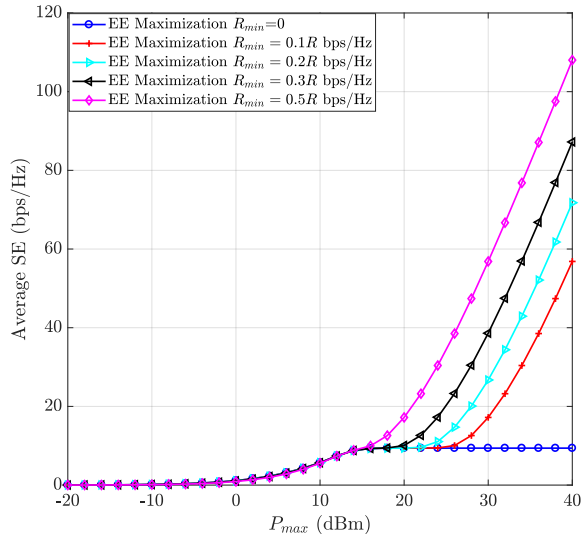


Figure 5. Average sum rate using LIS versus P_{\max} for $K = 16$, $M = 16$, $N = 32$, as well as different fractions of R for R_{\min} .

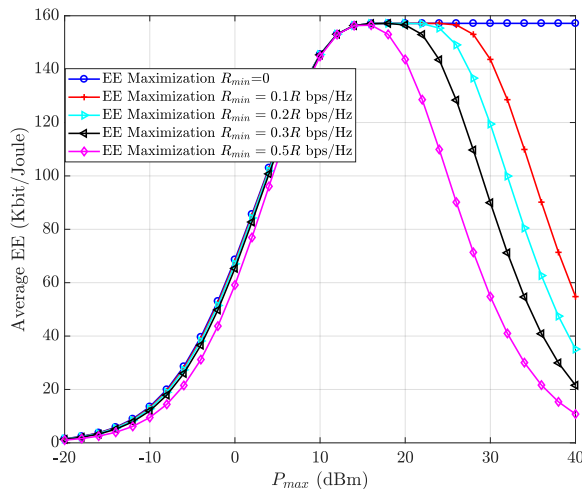


Figure 6. Average EE using LIS versus P_{\max} for $K = 16$, $M = 16$, $N = 32$, as well as different fractions of R for R_{\min} .

for larger P_{\max} , enforcing stricter QoS constraints causes the EE to decrease faster, due to the fact that the excess BS transmit power is used to meet the common user rate requirements.

D. Comparison between the Sum Rate and EE Maximizing Designs

In Figs. 7 and 8 we plot the average achievable sum rate and EE performances versus P_{\max} in dBm for the following design objectives: *i*) EE maximization with $R_{\min} = 0$ bps/Hz using Algorithm 2; *ii*) the same objective and algorithm with *i*) but with $R_{\min} = 0.2R$ bps/Hz; *iii*) sum rate maximization using the algorithm described in Section III-C; and *iv*) maximum power

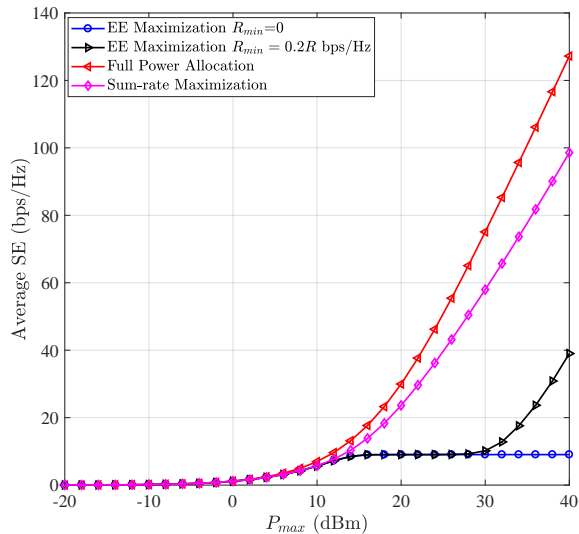


Figure 7. Average sum rate using LIS versus P_{\max} for $K = 16$, $M = 16$, and $N = 32$ using: a) our MM-based EE maximization algorithm for $R_{\min} = \{0, 0.2R\}$; b) full power allocation; and c) our sum rate maximization algorithm.

allocation P_{\max} to each user. It can be seen from both figures that all designs perform similarly for $P_{\max} \leq 15\text{dBm}$, which indicates that the EE and sum rate objectives are nearly equivalent for such transmit power levels. This can be explained by observing that for low P_{\max} , the EE is an increasing function of the BS transmit power, just as the sum rate is. In other terms, using full BS transmit power for low P_{\max} is optimal, and in this case, EE maximization reduces to sum rate maximization. However, as shown for $P_{\max} > 15\text{dBm}$, the EE maximizing objective and the sum rate one result in designs yielding substantially different performances. For such P_{\max} values, maximizing the sum rate requires utilizing all available BS power, whereas maximizing EE does require increasing the BS transmit power above a threshold value. As a result, the sum rate maximization design naturally increases the sum rate, but leads to decreasing EE. On the contrary, when maximizing EE both the achievable EE and sum rate performances become constant. It can be also observed from the results of Figs. 8 and 7 that, when EE is maximized subject to QoS constraints, an intermediate behavior is obtained due to the fact that some of the excess transmit power is used in order to fulfill the those constraints. Once the constraints are met, no further BS transmit power is needed.

E. Impact of the number of LIS Elements

In Fig. 9 we consider the gradient- and MM-based Algorithms 2 and 3, and demonstrate their achievable sum rate performances as functions of the number of the LIS reflecting elements N .

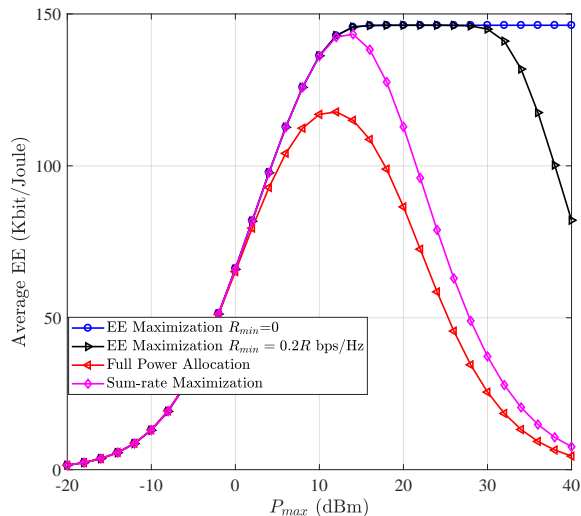


Figure 8. Average EE using LIS versus P_{\max} for $K = 16$, $M = 16$, and $N = 32$ using: a) our MM-based EE maximization algorithm for $R_{\min} = \{0, 0.2R\}$; b) full power allocation; and c) our sum rate maximization algorithm.

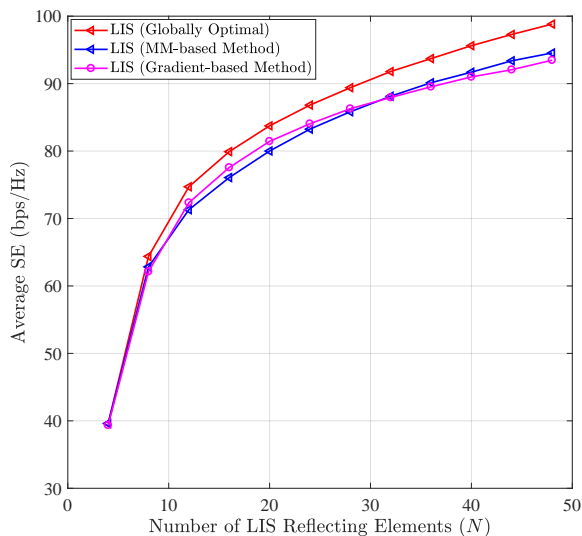


Figure 9. Average sum rate using LIS versus N for $\text{SNR} = 20\text{dB}$, $K = 16$, $M = 12$, and $R_{\min} = 2\text{bps/Hz}$ with both our presented algorithms as well as exhaustive global optimization.

We have set the transmit Signal Noise Ratio (SNR), defined as $\text{SNR} = P_{\max}/\sigma^2$, to 20dB using $\sigma^2 = 1$. In addition, we have used the parameter setting $K = 16$, $M = 12$, and $R_{\min} = 2\text{bps/Hz}$. In this figure, we also sketch the performance of the optimum sum rate design obtained by means of numerical global optimization, as described in Section (III-C). As clearly shown, both proposed algorithms yield very similar performance curves that are quite close to the ones obtained from the global optimization method. Furthermore, as expected, the larger the N value

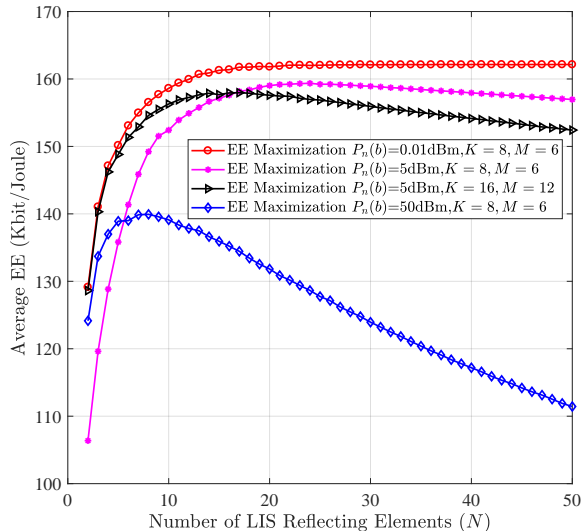


Figure 10. Average EE using LIS versus N for $\text{SNR} = -10\text{dB}$ and $R_{\min} = 0\text{bps/Hz}$, as well as: a) $P_n(b) = 0.01\text{dBm}$, $K = 8$, and $M = 6$; b) $P_n(b) = 5\text{dBm}$, $K = 8$, and $M = 6$; c) $P_n(b) = 5\text{dBm}$, $K = 16$, and $M = 12$; and d) $P_n(b) = 100\text{dBm}$, $K = 8$, and $M = 6$.

is, the larger is the achievable sum rate for the considered LIS-assisted system.

We finally plot the achievable EE performance using our MM-based Algorithm 2 in Fig.10 as a function of N . In this figure we consider the following cases for the number of users K , the number of BS antenna elements M , and the power consumption of each LIS b -bit phase resolution element: *i*) $P_n(b) = 0.01\text{dBm}$, $K = 8$, and $M = 6$; *ii*) $P_n(b) = 5\text{dBm}$, $K = 8$, and $M = 6$; *iii*) $P_n(b) = 5\text{dBm}$, $K = 16$, and $M = 12$; and *iv*) $P_n(b) = 100\text{dBm}$, $K = 8$, and $M = 6$. As observed, when N is quite small, i.e., $N \leq 5$, all designs exhibit the same trend. Particularly, EE performance increases as N increases. However, for a small-to-moderate N value and on, EE starts decreasing. This behavior seems not to happen for $P_n(b) = 0.01\text{dBm}$, but this is only due to the fact that this value of $P_n(b)$ is quite small, and thus it would take a very large N to observe EE decreasing. The results in Fig.10 confirm that there exists an optimal number N of LIS elements as far as the EE maximization objective is concerned. In other words, an optimal trade-off exists between the rate benefit of deploying larger and larger LIS structure and its corresponding energy consumption cost.

V. CONCLUSION AND FUTURE WORK

In this paper, we considered a LIS-assisted downlink multi-user MISO system and presented two computationally efficient EE maximization algorithms for the BS transmit power allocation

and the LIS reflector values. Both algorithms were based on alternating maximization, with the one adopting gradient descent for the LIS design, while the other is a MM-based approach. The optimal transmit power allocation was tackled by a fractional programming method. Special cases of both algorithms were used for the SE maximization design. Our numerical results showed that the proposed MM-based approach achieves near optimal SE performance, and that LIS-assisted communication can provide up to 300% higher EE than the relay-assisted one. It was also substantiated that the EE-optimal operating point depends on the numbers of mobile users and LIS elements, as well as the individual power consumption of the LIS elements. For future work, we intend to study the fundamental limits with LIS structures having realistically low resolution phase elements, and devise efficient LIS design algorithms capitalizing on practical channel acquisition techniques.

ACKNOWLEDGEMENT

The work of C. Yuen was supported by the MIT-SUTD International design center and NSFC 61750110529 Grant, and that of C. Huang by the PHC Merlion PhD program. The work of M. Debbah was supported by H2020 MSCA IF BESMART, Grant 749336, and H2020-ERC PoC-CacheMire, Grant 727682; the former project also funded the work of A. Zappone.

REFERENCES

- [1] C. Huang et al., "Achievable rate maximization by passive intelligent mirrors," in *Proc. IEEE ICASSP*, Calgary, Canada, Apr. 2018, pp. 1–6.
- [2] "NGMN alliance 5G white paper," [Online] <https://www.ngmn.org/5g-white-paper/5g-white-paper.html>, 2015.
- [3] Y. Chen et al., "Fundamental trade-offs on green wireless networks," *IEEE Commun. Mag.*, vol. 49, no. 6, pp. 30–37, Jun. 2011.
- [4] Ericsson White Paper, "More than 50 billion connected devices," Tech. Rep. 284 23-3149 Uen, Ericsson, Feb. 2011.
- [5] T. S. Rappaport et al., "Millimeter wave mobile communications for 5G cellular: It will work!," *IEEE Access*, vol. 1, pp. 335–349, 2013.
- [6] G. C. Alexandropoulos et al., "Advanced coordinated beamforming for the downlink of future LTE cellular networks," *IEEE Commun. Mag.*, vol. 54, no. 7, pp. 54–60, Jul. 2016.
- [7] J. Zuo et al., "Energy-efficient downlink transmission for multicell massive das with pilot contamination," *IEEE Trans. on Veh. Tech.*, vol. 66, no. 2, pp. 1209–1221, Feb 2017.
- [8] R. Mahapatra et al., "Energy efficiency tradeoff mechanism towards wireless green communication: A survey," *IEEE Commun. Surveys Tutorials*, vol. 18, no. 1, pp. 686–705, First quarter 2016.
- [9] S. Buzzi et al., "A survey of energy-efficient techniques for 5G networks and challenges ahead," *IEEE J. Sel. Areas Commun.*, vol. 34, no. 4, pp. 697–709, Apr. 2016.

- [10] A. Zappone and E. A. Jorswieck, "Energy efficiency in wireless networks via fractional programming theory," *Found. Trends in Commun. Inf. Theory*, vol. 11, no. 3–4, pp. 185–396, 2014.
- [11] S. V. Hum and J. Perruisseau-Carrier, "Reconfigurable reflectarrays and array lenses for dynamic antenna beam control: A review," *IEEE Trans. Antennas Prop.*, vol. 62, no. 1, pp. 183–198, Jan. 2014.
- [12] G. C. Alexandropoulos et al., "Precoding for multiuser MIMO systems with single-fed parasitic antenna arrays," in *Proc. IEEE GLOBECOM*, Austin, USA, Dec. 2014, pp. 3656–3661.
- [13] M. A. Sedaghat et al., "A novel single-RF transmitter for massive MIMO," in *Proc. WSA*, Erlangen, Germany, Mar. 2014, pp. 1–8.
- [14] F. Rusek et al., "Scaling up MIMO: Opportunities and challenges with very large arrays," *IEEE Signal Process. Mag.*, vol. 30, no. 1, pp. 40–60, Jan. 2013.
- [15] X. Gao et al., "Massive MIMO in real propagation environments: Do all antennas contribute equally?," *IEEE Trans. Commun.*, vol. 63, no. 11, pp. 3917–3928, Nov. 2015.
- [16] E. Björnson et al., "Massive MIMO systems with non-ideal hardware: Energy efficiency, estimation, and capacity limits," *IEEE Trans. Inf. Theory*, vol. 60, no. 11, pp. 7112–7139, Nov. 2014.
- [17] S. Hu et al., "Beyond massive mimo: The potential of data transmission with large intelligent surfaces," *IEEE Trans. Signal Process.*, vol. 66, no. 10, pp. 2746–2758, May 2018.
- [18] X. Tan et al., "Increasing indoor spectrum sharing capacity using smart reflect-array," in *Proc. IEEE ICC*, Kuala Lumpur, Malaysia, May 2016, pp. 1–6.
- [19] X. Tan et al., "Enabling indoor mobile millimeter-wave networks based on smart reflect-arrays," in *Proc. IEEE INFOCOM*, Honolulu, USA, Apr. 2018, pp. 1–9.
- [20] S. Foo, "Liquid-crystal reconfigurable metasurface reflectors," in *Proc. IEEE ISAP*, San Diego, USA, Jul. 2017, pp. 2069–2070.
- [21] C. Liaskos et al., "Using any surface to realize a new paradigm for wireless communications," [Online] <http://arxiv.org/abs/1806.04585>, 2018.
- [22] B. Sainath and N. B. Mehta, "Generalizing the amplify-and-forward relay gain model: An optimal SEP perspective," *IEEE Trans. Wireless Commun.*, vol. 11, no. 11, pp. 4118–4127, Nov. 2012.
- [23] J. Huang et al., "Relay beamforming for amplify-and-forward multi-antenna relay networks with energy harvesting constraint," *IEEE Signal Process. Lett.*, vol. 21, no. 4, pp. 454–458, Apr. 2014.
- [24] C. Chae et al., "MIMO relaying with linear processing for multiuser transmission in fixed relay networks," *IEEE Trans. Signal Process.*, vol. 56, no. 2, pp. 727–738, Feb. 2008.
- [25] A. Zappone et al., "Energy efficiency optimization in relay-assisted MIMO systems with perfect and statistical CSI," *IEEE Trans. Signal Process.*, vol. 62, no. 2, pp. 443–457, Jan. 2014.
- [26] R. W. Heath, Jr. et al., "A current perspective on distributed antenna systems for the downlink of cellular systems," *IEEE Commun. Mag.*, vol. 51, no. 4, pp. 161–167, Apr. 2013.
- [27] N. Kaina et al., "Shaping complex microwave fields in reverberating media with binary tunable metasurfaces," *Sci. Rep.* 4, pp. 1–7, Article No 076401, 2014.
- [28] N. Kaina et al., "Hybridized resonances to design tunable binary phase metasurface unit cells," *Opt. Express*, vol. 22, no. 16, pp. 1–8.
- [29] H. Yang et al., "A programmable metasurface with dynamic polarization, scattering and focusing control," *Sci. Rep.* 6, pp. 1–11, Article No 35692, 2016.
- [30] L. Subrt and P. Pechac, "Intelligent walls as autonomous parts of smart indoor environments," *IET Commun.*, vol. 6, no. 8, pp. 1004–1010, May 2012.

- [31] L. Subrt and P. Pechac, "Controlling propagation environments using intelligent walls," in *Proc. EUCAP*, Prague, Czech Republic, Mar. 2012, pp. 1–5.
- [32] C. Huang et al., "Energy efficient multi-user MISO communication using low resolution large intelligent surfaces," in *IEEE GLOBECOM*, Abu Dhabi, UAE, Dec. 2018, to appear, [Online] <http://arxiv.org/abs/1809.05397>.
- [33] Q. Wu and R. Zhang, "Intelligent reflecting surface enhanced wireless network: Joint active and passive beamforming design," in *IEEE GLOBECOM*, Abu Dhabi, UAE, Dec. 2018, to appear, [Online] <http://arxiv.org/abs/1809.01423>.
- [34] M. Dohler and Y. Li, *Cooperative communications: Hardware, channel & PHY*, Wiley, UK, 2010.
- [35] L. N. Ribeiro et al., "Energy efficiency of mmwave massive MIMO precoding with low-resolution DACs," *IEEE J. Sel. Topics Signal Process.*, vol. 12, no. 2, pp. 298–312, May 2018.
- [36] R. Méndez-Ria et al., "Hybrid MIMO architectures for millimeter wave communications: Phase shifters or switches?," *IEEE Access*, vol. 4, pp. 247–267, Jan. 2016.
- [37] S. Wagner et al., "Large system analysis of linear precoding in correlated MISO broadcast channels under limited feedback," *IEEE Trans. Inf. Theory*, vol. 58, no. 7, pp. 4509–4537, Jul. 2012.
- [38] G. C. Alexandropoulos, "Position aided beam alignment for millimeter wave backhaul systems with large phased arrays," in *Proc. IEEE CAMSAP*, Curaçao, Dutch Antilles, Dec. 2017, pp. 1–5.
- [39] A. Alkhateeb et al., "Deep learning coordinated beamforming for highly-mobile millimeter wave systems," [Online] <http://arxiv.org/abs/1804.10334>, 2018.
- [40] I. Csiszár and G. Tusnády, "Information geometry and alternating minimization procedures," *Statist. Decisions*, vol. 1, pp. 205–237, Dec. 1984.
- [41] L. Tang et al., "Fast algorithms for sparse frequency waveform design with sidelobe constraint," *Elsevier Digital Signal Process.*, vol. 69, pp. 140–153, 2017.
- [42] P. Stoica et al., "Optimization of the receive filter and transmit sequence for active sensing," *IEEE Trans. Signal Process.*, vol. 60, no. 4, pp. 1730–1740, Apr. 2012.
- [43] A. Zappone et al., "Globally optimal energy-efficient power control and receiver design in wireless networks," *IEEE Trans. Signal Process.*, vol. 65, no. 11, pp. 2844–2859, Jun. 2017.
- [44] D. R. Hunter and K. Lange, "A tutorial on MM algorithms," *American Stat.*, vol. 58, no. 1, pp. 30–37, 2004.
- [45] Y. Sun et al., "Majorization-Minimization algorithms in signal processing, communications, and machine learning," *IEEE Trans. Signal Process.*, vol. 65, no. 3, pp. 794–816, Feb. 2017.
- [46] J. Song et al., "Optimization methods for designing sequences with low autocorrelation sidelobes," *IEEE Trans. Signal Process.*, vol. 63, no. 15, pp. 3998–4009, Aug. 2015.
- [47] T. Abrudan et al., "Conjugate gradient algorithm for optimization under unitary matrix constraint," *Elsevier Signal Process.*, vol. 89, no. 9, pp. 1704–1714, 2009.
- [48] D. Zhao et al., "Spectrum optimization via FFT-based conjugate gradient method for unimodular sequence design," *Elsevier Signal Process.*, vol. 142, pp. 354–365, 2018.
- [49] J. Liang et al., "Unimodular sequence design based on alternating direction method of multipliers," *IEEE Trans. Signal Process.*, vol. 64, no. 20, pp. 5367–5381, Oct. 2016.
- [50] O. Aldayel et al., "Tractable transmit MIMO beampattern design under a constant modulus constraint," *IEEE Trans. Signal Process.*, vol. 65, no. 10, pp. 2588–2599, May 2017.
- [51] L. Wu et al., "Cognitive radar-based sequence design via SINR maximization," *IEEE Trans. Signal Process.*, vol. 65, no. 3, pp. 779–793, Feb. 2017.
- [52] E. Björnson et al., "Optimal design of energy-efficient multi-user MIMO systems: Is massive MIMO the answer?," *IEEE Trans. Wireless Commun.*, vol. 14, no. 6, pp. 3059–3075, Jun. 2015.